Development of Three-Dimensional Icing Simulation Code for Wind Turbines

Chankyu Son[1], Holger Koss[1], Taeseong Kim[1,2]

[1] *Technical University of Denmark, Denmark*
[2] *School of Mechanical, Electrical and Manufacturing Engineering, Loughborough University, UK*

cson@win.dtu.dk, hko@byg.dtu.dk, tkim@win.dtu.dk

Abstract— **This study aims to develop a three-dimensional icing simulation code for wind turbines under various icing conditions named WISE (Wind turbine Icing Simulation code with performance Evaluation). In order to explain the rotating wind turbines, the Moving Reference Frame (MRF) method is applied for both aerodynamic and droplet fields. The thin water film model plays a role to predict the motion of the water film is applied in the thermodynamic module. The ice accretion shapes on NREL Phase VI were obtained by using WISE under rime and glaze ice conditions. The ice accretion shapes were qualitatively compared against FENSAP-ICE, the state-of-the-art program. For rime ice condition, the icing limits, maximum thickness and its location of WISE are well matched with those of FENSAP-ICE. For glaze ice condition, there are discrepancies of icing limits. On the suction side, the results of WISE with high accuracy flow field calculation are expected to be valid. However, WISE underestimates the mass of ice on the pressure side. To improve the accuracy for the pressure side, the turbulence model, currently a fully turbulence model, is considered, will be investigated.**

Keywords— ***Moving reference frame, Wind turbine icing, Glaze ice, Navier-Stokes equations, NREL Phase VI***

I. INTRODUCTION

Cold regions have low temperate with high density make the energy potential. Therefore, wind farms are in operation or planning in cold climates: Northern and Central Europe, Northern America and Asia [1]. However, icing events are inevitable for cold regions which poses a significant challenge to wind energy harvesting in those areas.

Wind turbine icing occurs when super-cooled droplets impact upon the wind turbine blades and freeze on the surface. According to meteorological variables such as temperature, humidity, Median Volume Diameter (MVD), and so on, the types of ice can be determined as rime and glaze ice.

Rime ice can be expected under low temperature (below -10 to -15℃) and humidity conditions. Since the impinged droplets become ice immediately, the ice shapes are similar to underlying blade shapes. In addition, this type of ice is opaque because it includes air pockets inside. On the other hand, some impinged droplets form thin water layer which follows along the surface and freezes on a specific region where the heat convection rate is high in high humidity and temperature. This is categorized by glaze ice. The ice horn shape is the representative feature of glaze ice. Since the flow separation arises behind the ice horn, the aerodynamic penalty is relatively high. This severe icing event makes the turbine load increase, and eventually leads to a complete loss of production [1].

It is important to predict the accurate icing shapes on the wind turbine under various metrological conditions. The generated power drops can be estimated due to short-term icing events. Moreover, wind farm site analysis is possible for evaluating the aerodynamic performance of the ice accumulated blades from the long term weather forecast. In addition, the predicted ice accretion shapes on wind turbine blades are basis information to design icing detection systems and efficient anti/de-icing devices based on which include the information of the covered area and total mass of ice for wind turbines.

Due to the development of computational techniques, numerical icing simulations such as estimation of ice accretion shapes and examination of aerodynamic performances have been widely used. In the early 1980s, two-dimensional ice accretion solvers were developed in NASA, ONEARA, DRL, and CIRA for the aircraft icing research [2]. After that, it started to be used in wind turbine icing as well [3].The early stage of icing simulations adopted panel method or Euler equation solvers with boundary layer theory as the aerodynamic solver. For tracking the water droplets, Lagrangian approaches were mainly applied. Messinger model [4] to predict the phase change of the impinging water was applied. Because two-dimensional icing simulations were extended based on blade element theory (BET), the effects of rotational motion and wake were not able to be considered. Lagrangian approach was not accurate to predict trajectories of droplets near the blade tip region where the three-dimensional effect cannot be ignored. Two-dimensional based solver cannot explain spanwise runback water. In addition, the inviscid assumption had limitations to estimate the penalty of generating power due to ice accretion.

To this end, there were some attempts to consider the three-dimensional effects with the blade rotation based on Navier-Stokes equations. Reid, T., *et al.* [5] performed three-dimensional icing simulations on NREL phase VI by using FENSAP-ICE which is widely used in the in-flight icing community for aircraft. They also systematically evaluated the performance of ice accumulated blades with various icing conditions by including the thermodynamic module. Although their study represented one of the first applications of FENSAP-ICE to a wind turbine, it is not clear how the detailed models were extended from fixed-wing aircraft to rotating wind turbines.

Hu, L., *et al.* [6] suggested a three-dimensional icing simulation code for rime ice conditions. They predicted ice shapes and extracted the quantitative power, which is generated under icing conditions on NREL phase VI wind

turbine. They applied a Moving Reference Frame (MRF) model for the aerodynamic module to consider the rotational effect of blades. However, droplet field module follows the method for fixed-wing aircraft.

Wang, Z. *et al.* [7] applied MRF method for both aerodynamic and droplet field modules, and then they add a thermodynamic model which can explain the phase change of the water film induced by impinged water droplets. They can explain ice accretion shapes on blades under both rime and glaze icing conditions. They clearly described a procedure and methodologies to predict ice accretion shapes for the rotating problem. However, boundary layer theory which requires streamwise directions is applied for a thermodynamic module. It has limitation to apply in conditions when flow separation is caused by high angle of attack or ice horn.

This study focus on the development of three-dimensional icing simulation code which is consistently considered the effects of blade rotation. To this end, the MRF method is applied for the aerodynamic module based on Reynolds Averaged Navier-Stokes (RANS) equations. Eulerian approach is also used by following the MRF method for droplet field module. Thin water film model is employed to explain the amount and directions of runback water. The shear force of air, the driving force of water film, was obtained from not boundary layer theory but RANS based aerodynamic solver.

The developed solver has been qualitatively validated against the results from other numerical simulations because there are few available experimental data for the three-dimensional wind turbine ice accretion. NREL Phase VI was chosen as a target wind turbine. The feature of the developed solver was analysed under rime and glaze ice conditions.

II. Numerical Method

The structure of Wind turbine Icing Simulation code with performance Evaluation (WISE) is shown in Fig. 1. WISE is extended from the fixed-wing aircraft icing tool named ISEPAC [8]. WISE consists of four parts: 1) flow analysis module, 2) droplet-trajectory calculation module, 3) thermodynamic module, and 4) grid-regeneration module.

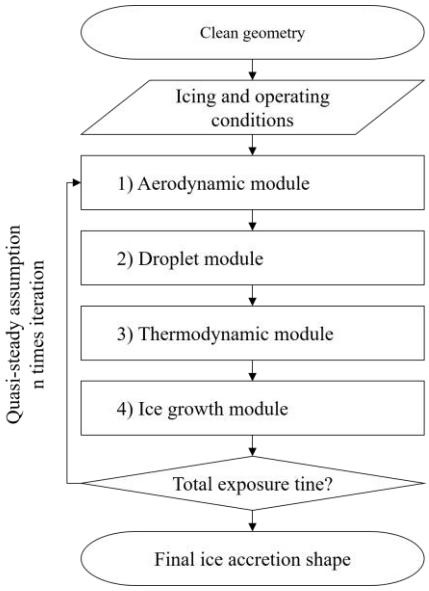

Fig. 1 Flow chart of the developed code.

All of the modules were developed on the single platform, OpenFOAM® v1712, rendering the user inconvenience minimal with respect to the data transfer between the modules. Moreover, extensive parallel computing involving the present icing-analysis package could be performed because OpenFOAM itself supports OpenMPI-based parallel computing [9].

The icing phenomenon occurs from several minutes to several hours. It is impossible to predict ice accretions shapes through the entire modules under unsteady simulations. For the time being, in this study, quasi-steady flows are assumed because of limited computational resources. By using the converged velocity vectors obtained from the flow analysis module, droplet trajectories are computed. Then, using these results, the thermodynamic analyses are performed. Finally, the ice shapes are explicitly determined from the evaluation of the ice mass accreted on the surface.

The current WISE assumes rigid structures. The effect of structural vibrations and bending of the blades due to gravity are neglected.

A. Aerodynamic Module

rhoPimpleFoam [9] with the MRF model is chosen for the aerodynamic module for WISE. rhoPimpleFoam with MRF solves compressible RANS equations under a steady-state approximation.

Although the steady-state approximation of the MRF model cannot explain the turbulence of freestream and blade pitching motions, it is beneficial to reduce computation times while considering the blade rotation. Because the exposure time is very long, changes of turbulence and blade pitching in short periods can be ignored.

The calculated results of compressible RANS equations are used in WISE. In particular, the aerodynamic module in WISE is in charge of determining the directions of runback and heat transfer between the surface and unfreezing water. The driving force of runback water is the shear of air. The conservation of momentum implements the shear force of air, hence allowing for calculating the effect from blade rotation. The heat transfer rate was calculated using the temperature gradient from the energy equation. This information is delivered to the thermodynamic module.

Once the ice is accumulated on the surface, the surface roughness is increased. Because the flow changes to fully developed turbulent flow on the roughened surface, it can be assumed that the flow is completely turbulent. To account for the wall roughness, the modified Spalart–Allmaras turbulence model [10] is applied.

The surface roughness is dependent on the ambient temperature, liquid water content (LWC), MVD, and velocity. In this study, the more advanced surface-roughness model developed by NASA LEWICE was applied [11], where the surface roughness is given as a function of the temperature, velocity, LWC, MVD, and chord length. A constant roughness value is applied along the blades to avoid iterative calculations. Here, the information of 75% span is used as the representative location.

B. Droplet Field Module

The droplet field module determines the mass of the droplets that are collected on the surface. The Eulerian

approach is applied because of its superiority when considering the icing phenomenon under massive separation. Additionally, the same grid system with the aerodynamic module can be used to calculate the droplet fields.

The droplet field was calculated based on the converged velocity vectors in the aerodynamic module, and for the computation, the mass and momentum conservation equations were used, as shown in Eqns. (1) and (2), respectively:

$$\frac{\partial \bar{\rho}_d}{\partial t} + \nabla \cdot \left(\bar{\rho}_d \vec{u}_{d,r}\right) = 0 \tag{1}$$

$$\begin{aligned} &\frac{\partial \bar{\rho}_d \vec{u}_{d,r}}{\partial t} + \nabla \cdot \left(\bar{\rho}_d \vec{u}_{d,r} \vec{u}_{d,r}\right) + 2\bar{\rho}_d \omega \times \omega \times \vec{r} \\ &+\omega \times \vec{u}_{d,r} = \frac{3}{4} \frac{\bar{\rho}_d \mu_a C_D Re_d}{\rho_w MVD^2} \left(\vec{u}_{a,r} - \vec{u}_{d,r}\right) \end{aligned} \tag{2}$$

The drag coefficient (C_D) on the droplet was used, as in Eq. (3).

$$C_D = \frac{24}{Re_d}\left(1 + 0.197 {Re_d}^{0.63} + 2.6 \times 10^{-4} {Re_d}^{1.38}\right) \tag{3}$$

The boundary conditions were imposed based on the relation between the relative droplet velocity vector ($\vec{u}_{d,r}$) and the surface normal vector ($\vec{n}$), which is written as:

$$\vec{u}_{d,r} \cdot \vec{n} > 0, \vec{u}_{d,r} = \vec{u}_d, \bar{\rho}_{d,r} = \bar{\rho}_d \tag{4}$$

$$\vec{u}_{d,r} \cdot \vec{n} < 0, \vec{u}_{d,r} = 0, \bar{\rho}_d = 0 \tag{5}$$

The collection efficiency (β) is determined based on the computed velocity vector and bulk density ($\bar{\rho}_d$) as shown in Eq. (6). It is normalized by velocity (U_∞) and liquid water contents (LWC_∞) of freestream. The centrifugal and Coriolis forces are added in the momentum equation as source terms. It does not require a specific calibration or model to impose the effects of blade rotation. As the result, the mass flow rate of impinging water ($\dot{m}_{com}$) can be calculated as defined in Eq.(7).

$$\beta = \frac{\bar{\rho}_d \vec{u}_{d,r} \cdot \vec{n}}{LWC_\infty \cdot U_\infty} \tag{6}$$

$$\dot{m}_{com} = \beta LWC_\infty \cdot U_\infty \tag{7}$$

C. Thermodynamic module

The mass of freezing ice and runback water can be determined by the thermodynamic module. On the blade surface, mass, momentum and energy conservation laws are imposed in WISE. However, some of the terms have been modified as part of efforts to consider rotational motion.

First, shear force of air ($\vec{\tau}_{w,r}$) is calculated by the relative velocity from the aerodynamic module. The momentum conservation can be abbreviated under the thin water film theory [12] as written in Eq. (8). It was assumed that the driving force acting on the thin water film is the shear force of air. The directions of runback water are only determined by the shear force of air. Since the centrifugal and Coriolis forces are added in aerodynamic module, the effect of rotation is indirectly reflected by the motion of thin water film.

$$\bar{U}_f = \frac{1}{h_f}\int_0^{h_f} u_f dh = \frac{h_f}{2\mu_w}\vec{\tau}_{w,r} \tag{8}$$

The assumption to explain the motion of water film is valid for small scale wind turbine with low rpm. The radius of angular momentum cannot be ignored as increasing the radius of wind turbines such as the tip region of full scale wind turbines. The centrifugal and Coriolis forces should be considered directly to the momentum conservation of water film.

The shear force is already known from the flow solver, and the other unknowns, such as the water-film thickness, ice mass, and surface temperature, can be determined based on the mass and energy conservation equation.

Equation (9) is the mass conservation equation. For the mass conservation, the mass flow rate of impinging water ($\dot{m}_{com}$) is applied.

$$\rho_w \left[\int \frac{\partial h_f}{\partial t} dV + \int \nabla \cdot \left(h_f \bar{U}_f\right) dV\right] = \dot{m}_{com} - \dot{m}_{ice} \tag{9}$$

As the efforts to consider the rotation of the blade, the energy conservation which is written in Eq. (10) is modified. The first term of right-hand side means the kinetic energy of the impinging water droplets to the surface. The relative velocity of water droplet is applied. In addition, the heat convection coefficient (h_c) is obtained from the aerodynamic module which is based on the MRF model.

$$\begin{aligned} &\rho_w \left[\int \frac{\partial h_f c_{p,w} \tilde{T}_{eq}}{\partial t} dV + \int \nabla \cdot \left(h_f c_{p,w} \tilde{T}_{eq} \bar{U}_f\right) dV\right] \\ &= \dot{m}_{com}\left[c_{p,w}\tilde{T}_{d,\infty} + \frac{1}{2}U_{d,r}^2\right] \\ &\quad + \dot{m}_{ice}\left[L_{fus} - c_{p,i}\tilde{T}_{eq}\right] + h_c\left(T_{eq} - T_\infty\right) \end{aligned} \tag{10}$$

There are three unknowns in the previous equations, namely the ice mass ($\dot{m}_{ice}$), water-film thickness (h_f), and surface temperature ($\tilde{T}_{eq}$). These unknowns are less than the number of equations, therefore they cannot be uniquely determined. To determine the unknowns, an additional relation proposed by Messinger was used [4]. First, the state of the surface from the Messinger model was assumed, and then the mass- and energy-conservation equations were solved. Finally, the physically valid state of the surface was determined by the following method.

Fig. 2 shows the sequence to find the correct surface conditions. When the surface temperature is above the 0°C, pure water exists on the surface which means that the mass of freezing ice should be zero. The thickness of water film can be calculated from mass conservation. Then the temperature of the surface can be determined by the energy conservation. If the heat convection rate varies with the latent heat of fusion,

water is assumed to coexist with ice on the surface. The surface temperature is set to freezing temperature. Lastly, when the heat transfer rate is dominant, there is no water on the surface.

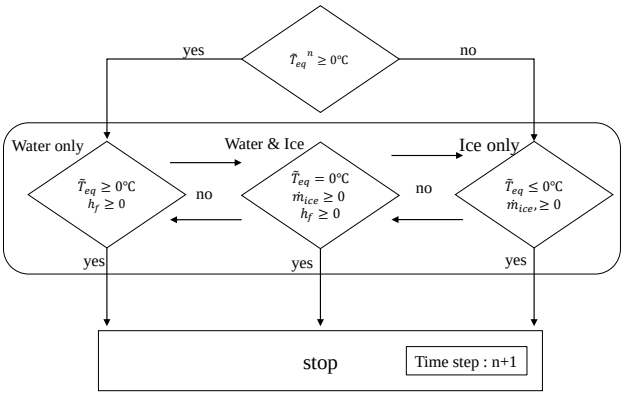

Fig. 2 Flow chart of the thermodynamic model.

D. *Ice growth module*

The ice growth module of WISE is the same as that of ISEPAC. From the calculated mass of ice, the thickness is determined as shown in Eq. (11). The ice density was set to 920 kg/m³.

$$h_t = \frac{\dot{m}_{ice}\Delta t}{\rho_{ice} A_{sur}} \tag{11}$$

III. Results and Discussion

A. *Aerodynamic Module*

The compressible MRF model for wind turbines was verified by experimental and numerical methods. The NREL phase VI was chosen as the validation model. The NREL phase VI rotor consists of two blades, each 5m in span. The tapered and twisted blades are based on the S809 airfoil described by Giguère and Selig [13]. The wind speed is 7m/s and rotational speed is 72 rpm.

Sectional pressure distributions are illustrated in Fig. 3. Numerical results obtained by FENSAP-ICE [5], FLUENT [6], and the present method are compared with the experiment which was performed by using NASA Ames 80ft × 120ft wind tunnel [14].

To validate the aerodynamic module, the present method is performed under ambient and pressure conditions. The MRF model is applied based on compressible RANS equations. Spalart-Allaras model is applied as the turbulence model without surface roughness. 5.5 million grid cells are used with a cylindrical computational domain.

As shown in Fig. 3, present method and FLUENT which is performed by Lu H. *et al.* [6] are well matched with experiment not only at the inboard (r/R = 46.7%) but as near the tip region (r/R=80%). Lu, H. *et al.* used incompressible solver with k-ω SST as the turbulence mode. Although, the present method and FLUENT numerical simulations have differences to calculate the flow field, both simulations are performed under fully turbulent assumption without any transition model from laminar to turbulent.

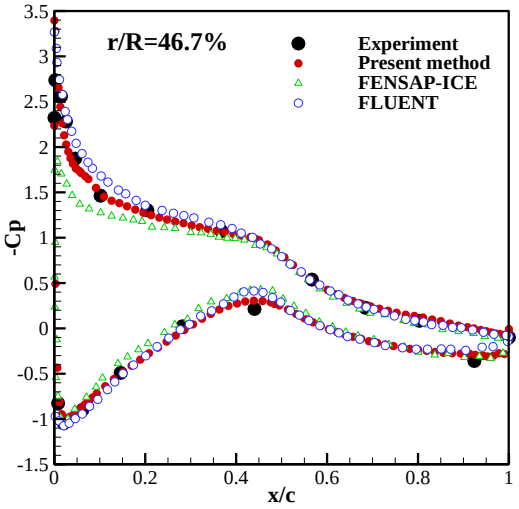

(a) r/R = 46.7%

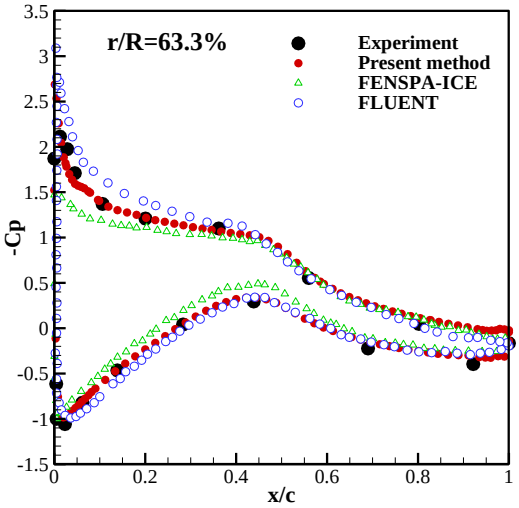

(b) r/R = 63.3%

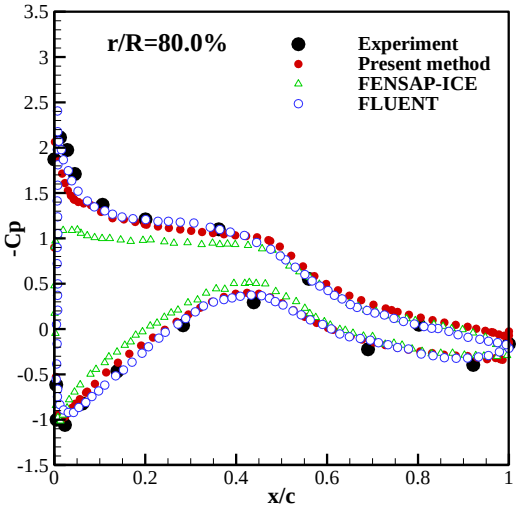

(c) r/R = 80%

Fig. 3 Sectional pressure distributions; Experiment [14], present method, FENSAP-ICE [5], and FLUENT [6].

FENSAP-ICE, however, yields lower suction peaks at all locations. FENSAP-ICE also employs the MRF method, but the free transition model has been activated for the flow simulations over the clean and uncontaminated rotor [5]. The pressure distributions on the suction side are flat. In particular, it becomes even more flat above 63.3%, as if leading edge separation had occurred. It can be expected that momentum was not transferred in the laminar region.

NREL Phase VI which is the scaled model has 5m radius. The free transition model seems reasonable since Reynolds number at r/R=75% is above 1.7×10^6. Moreover, ice roughness immediately triggers the transition to turbulent flow on the blades' surface. Irrespective of turbulence model, fully turbulence assumption yields accurate results for icing simulations of NREL Phase VI.

B. Droplet Field Module

The droplet field module was verified by comparing the ice accretion shapes under the rime ice assumption as shown in Table 1. Due to the absence of reliable experimental results for ice accretion shapes and collection efficiency on NREL Phase VI, numerical results are compared under the rime ice condition.

TABLE 1 VALIDATION CONDITIONS.

Types	Rime	Glaze
T_∞ [K], [°C]	258, -15.15	273.15, -3
U_∞[m/s]	7	7
Rotational speed [RPM]	72	72
LWC [g/m³]	0.5	0.5
MVD [μm]	20	20
Time [m]	60	60

If the ambient temperature is low enough, the water droplets freeze immediately without runback water. The mass of impinging water is identical to the freezing ice. Under the rime ice conditions, the local ice thickness is proportional to collection efficiency. Therefore the ice accretion shapes on the wind turbine are depicted in Fig 4. To simulate rime ice condition, the thermodynamic module was deactivated.

Droplet trajectories can be determined by the predicted flow fields and drag force acting on water droplet. However, centrifugal and Coriolis forces are the most important terms in the momentum conservation of droplet field for the rotating problem.

Hu, *et al.* [6] used the MRF method for the flow field. Then the calculated vectors of air are imposed to obtain drag force on the droplet calculated from the relative velocity between the air and droplet fields as shown in Eq. (2). However, centrifugal and Coriolis forces are omitted in the momentum conservation of the droplet field, resulting in increasing the momentum of the flow field. Finally, they calculate the collection efficiency by using absolute droplet velocity ($\vec{u}_{a,d}$), and then the collection efficiency is correlated by adding angular velocity of the droplet field as written in Eq. (12). As a consequence, the thickness of ice is overestimated.

$$\beta = \frac{\bar{\rho}_d \vec{u}_{a,d} \cdot \vec{n}}{LWC_\infty \cdot U_\infty} + \frac{\bar{\rho}_d \cdot \vec{\omega} \times \vec{r} \cdot \vec{n}}{LWC_\infty \cdot U_\infty} \tag{12}$$

On the other hand, both flow and droplet fields are applied by the MRF method in this study. Without any correlations, the collection efficiency is predicted by Eq. (6). As a result, the ice accretion shapes predicted by WISE are similar to the ones obtained by FENSAP-ICE under rime ice conditions shown in Fig. 4. The quantitative shape parameters for rime ice shapes are icing limits, maximum thickness, and the ice growth direction.

The maximum ice thickness mainly appears at the stagnation point under rime ice conditions. The ice grows in the opposite direction of flow. The magnitude of velocity for the droplet field should be accurately predicted. Both results obtained by the present method and FENSAP-ICE are well matched for the maximum thickness and the direction of ice growth except for the tip region (r/R = 80%).

Impinging limits are identical to icing limits because there is no runback water under the rime ice conditions. Near the impinging limits, the surface normal vector and the velocity vector of the droplet field are perpendiculars. Therefore, the direction of droplet field should be predicted correctly as well. The impinging limits from the present method also well agree with the results of FENSAP-ICE. At the tip region (r/R = 80%), the impinging limits on both surfaces are shifted toward the trailing edge.

The difference of the quantitative shape parameters at the tip region is related to the results of the aerodynamic module. Both numerical simulations have different pressure distributions. As can be seen in Fig. 3 (c), FENSAP-ICE predicts leading edge separation. The slower velocity fields for air and droplet can be expected in FENSAP-ICE. It generates lower collection efficiency and droplet inertia. Finally, the small ice thickness at the stagnation point and icing limits shifted toward the trailing edge were predicted in FENSAP-ICE near the tip region.

C. Ice Accretion Shapes under the glaze condition

To verify the thermodynamic module, the glaze ice condition as written in Table 1 has been investigated. There are few numerical results for three-dimensional ice accretion shapes on rotating wind turbines under glaze ice conditions. The ice accretion shapes on NREL phase VI obtained by WISE are depicted with FENSAP-ICE [5].

Fig. 5 shows the ice accretions shapes between WISE and FENSAP-ICE. It is clearly seen that the icing limits on both surfaces and ice thickness on the pressure side are not matched well. The ice-covered area of the glaze ice condition predicted by FENSAP-ICE [5] is wider than the rime ice case shown in Fig. 4. It might be that the unfrozen water flows toward trailing by following the shear force of air as written in Eq. (8). However, for the present method predicted by WISE the flowing runback water from the stagnation point to the trailing edge is prevented due to the high adverse pressure gradient. As it is shown in Fig. 3, the pressure gradient predicted by WISE is higher than FENSAP-ICE on the suction side at all sections. The air loses their momentum before impinging limits. It makes that the runback water was stayed before impinging limits in WISE unlike FENSAP-ICE. Thus, the icing limits for both simulations have a discrepancy.

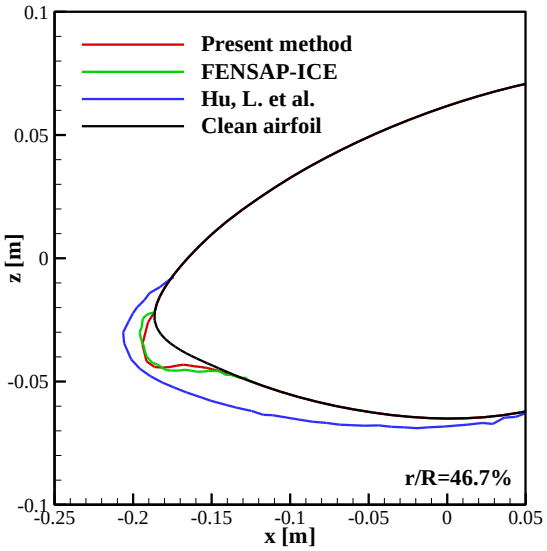

(a) r/R = 46.7%

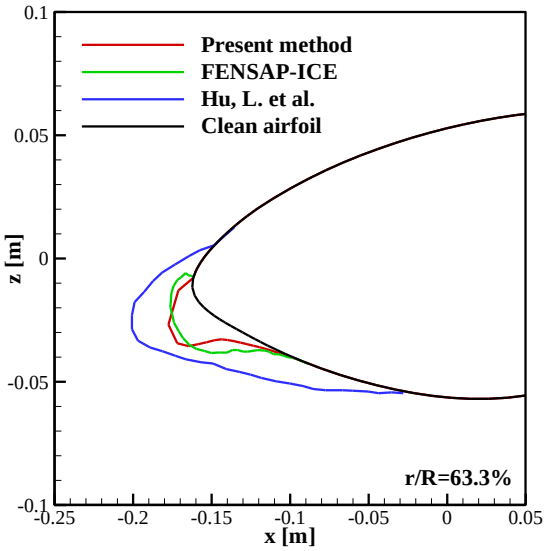

(b) r/R = 63.3%

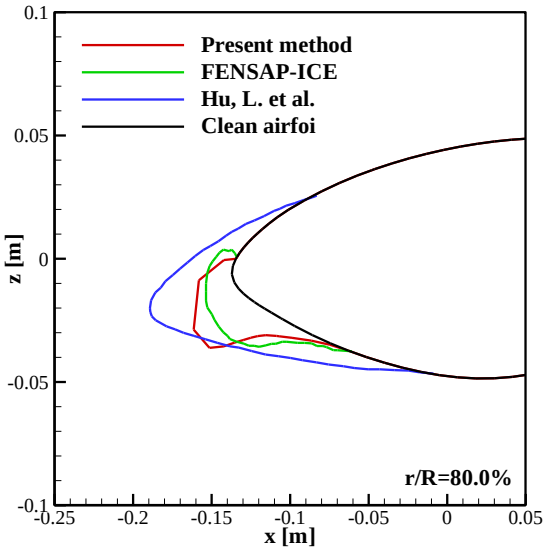

(c) r/R = 80%

Fig. 4 Sectional ice accretion shapes under rime ice condition; present method, FENSAP-ICE [5], and Hu, L. [6].

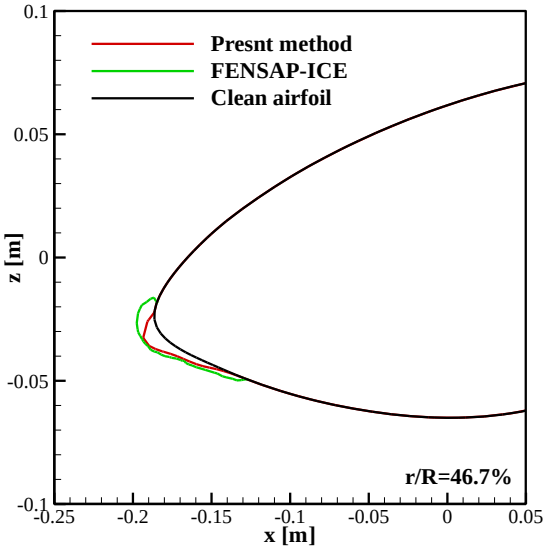

(a) r/R = 46.7%

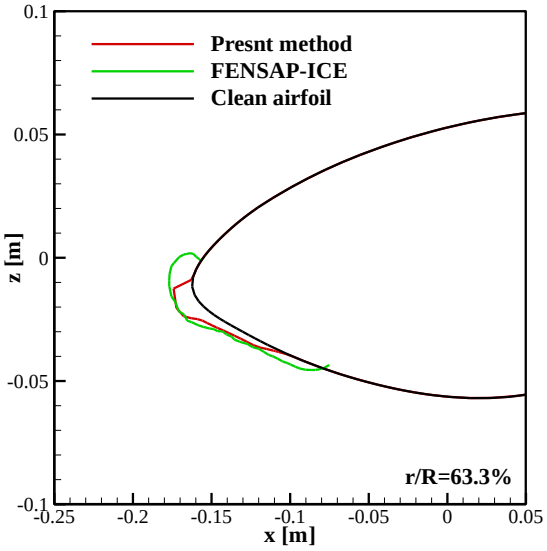

(b) r/R = 63.3%

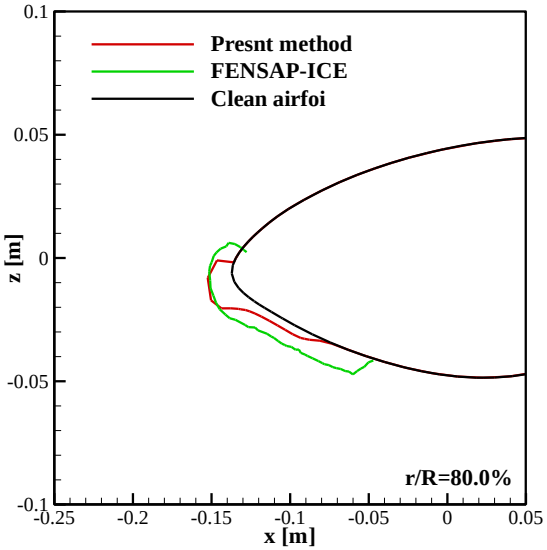

(c) r/R = 80%

Fig. 5 Sectional ice accretion shapes under glaze ice condition; present method and FENSAP-ICE [5].

It appears that WISE underestimates the ice thickness on the pressure side. Since the ice thickness is determined by the heat transfer rate which is calculated from the aerodynamic module, the difference might be introduced by the flow model. FENSAP-ICE applied the free transition model, whereas WISE assumed fully turbulent. In order to clarify the effect of the flow transition the heat transfer rate is compared with LEWICE [11] where NACA0012 with the chord length of 0.5334m, the angle of attack of 4°, freestream velocity of 102.8m/s and temperature of 262.04K are considered, respectively. Fig. 6 shows the heat transfer rate comparison between WISE and LEWICE. The horizontal axis means the distance from the stagnation point along the airfoil surface. The positive value is the suction side and the negative means pressure side.

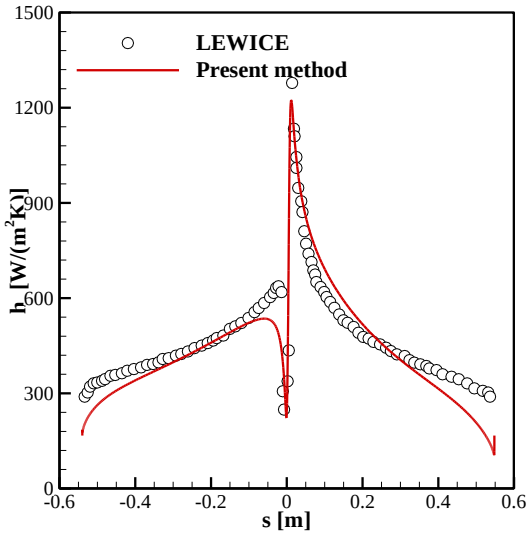

Fig. 6 Convective heat transfer rate on NACA0012 airfoil; present method and NASA LEWICE [11].

The heat transfer rate of WISE is well matched with LEWICE on the suction side. The high speed on the upper surface accelerates the flow transition from laminar to turbulent. Thus, the assumption of fully turbulent is reliable. On the other hand, the flow transition is impeded due to the relatively low velocity on the pressure side. Laminar flow keeps a certain area without flow trnasition. The heat transfer rate can be observed in the laminar region. It seems necessary using the transition model to improve the accuracy on the pressure side. WISE will be updated by adding the transition model with surface roughness recently applied in OVERFLOW2 [15].

IV. Concluding Remarks

In the present study, the up-to-date numerical analysis program WISE (Wind turbine Icing Simulation code with performance Evaluation) was developed for three-dimensional wind turbines. In order to include the blade rotation, the MRF method is applied for aerodynamic and droplet fields. The thermodynamic module based on the thin water film model is employed to determine the directions of unfreezing water under glaze ice conditions. The developed simulation program was qualitatively compared against FENSAP-ICE, the state-of-the-art program. The icing simulations were applied for NREL Phase VI under the rime and glaze ice conditions. Through a series of computations, the following conclusions are drawn.

The MRF method should be applied for air and droplet fields. When the collection efficiency is correlated by adding the angular velocity, the ice accretion shapes can be overestimated. However, WISE accurately predict the rime ice shape by applying the MRF method to the droplet field without any correlations.

WISE can predict three-dimensional the glaze ice shapes by adding thermodynamic module based on thin water film theory. The ice-covered area of WISE is narrower than that of FENSAP-ICE. On the suction side, the results of WISE with high accuracy of flow field calculation are expected to be valid. However, WISE underestimate the mass of ice on the pressure side. It is necessary to improve the turbulence model which can predict the flow transition.

Nomenclature

A_{sur}	=	*surface area, m2*
β	=	collection efficiency
c	=	characteristic length, m
h_c	=	heat convection coefficient, W/m^2·K
C_D	=	drag coefficient
C_p	=	specific heat
c_p	=	pressure coefficient
Δt	=	exposed time in icing condition, s
h_f	=	height of water film, m
h_t	=	height of ice, m
k_s	=	surface roughness, m
L_{fus}	=	latent heat of fusion, 334 kJ/kg
LWC	=	liquid water contents, g/m^3
MVD	=	median volume diameter, μm
μ_a	=	viscosity of air, Pa·s
$\dot{m}_{com}$	=	impinging water rate, kg/s
$\dot{m}_{ice}$	=	accumulated ice rate, kg/s
$\vec{n}$	=	outward normal vector of surface
ω	=	angular velocity, rad/s
R	=	rotor radius, m
r	=	sectional radius, m
$\vec{r}$	=	position vector, m
Re_d	=	droplet diameter based Reynolds number
ρ	=	density, g/m^3
$\bar{\rho}$	=	bulk density, g/m^3
s	=	distance from stagnation, m
t	=	time, s
T	=	temperature, K
$\tilde{T}_{eq}$	=	equilibrium temperature, ℃
$\vec{\tau}_w$	=	shear stress on the water film from air, Pa
U	=	velocity, m/s
$\vec{u}$	=	velocity vector, m/s
$\bar{U}_f$	=	mean velocity of water film, m/s

sub

a	=	air properties, absolute frame
d	=	droplet properties
i	=	ice properties
∞	=	freestream properties
r	=	relative frame
w	=	water properties

ACKNOWLEDGMENT

The work was supported financially by IEA Task 19 project (EUDP Grant 64016-0077)

REFERENCES

[1] T. Laakso, I. Baring-Gould, M. Durstewitz, R. Horbaty, A. Lacroix, E. Peltola, G. Ronsten, L. Tallhaug, and T. Wallenius, "State-of-the-Art of Wind Energy in Cold Climates," VTT, No. 1459-7683, 2010.

[2] W. B. Wright, R. W. Gent, and D. Guffond, "DRA/NASA/ONERA Collaboration on Icing Research Part Ⅱ -Prediction of Airfoil Ice Accretion," NASA CR-202349, 1997.

[3] W. Jasinski, S. Noe, M. Bragg, "Wind turbine performance under icing conditions," *In 35th Aerospace Sciences Meeting and Exhibit*, 1997, AIAA Paper 97-0977.

[4] B. L. Messinger, "Equilibrium Temperature of an Unheated Icing Surface as a Function of Air Speed," *Journal of the Aeronautical Sciences*, vol. 20, no. 1, pp. 29–42, 1953.

[5] T. Reid, G. Baruzzi, I. Ozcer, D. Switchenko, and W. Habashi "FENSAP-ICE simulation of icing on wind turbine blades, part 1: performance degradation," *In 51st AIAA aerospace sciences meeting including the new horizons forum and aerospace exposition*, 2013, AIAA paper 2013-0750.

[6] L. Hu, X. Zhu, J. Chen, X. Shen, and Z. Du, "Numerical simulation of rime ice on NREL Phase VI blade," *Journal of Wind Engineering and Industrial Aerodynamics*, vol. 178, pp. 57-68, July, 2018.

[7] Z. Wang, and C. Zhu, "Numerical simulation for in-cloud icing of three-dimensional wind turbine blades," *Simulation: Transactions of the Society for Modeling and Simulation International*, vol. 94, no. 1, pp. 31-41, 2018.

[8] C. Son, K. Yee, "Procedure for Determining Operation Limits of High-Altitude Long-Endurance Aircraft Under Icing Conditions," Journal of Aircraft, vol. 55, No. 1, pp. 294-309, 2017.

[9] (2017) Open-source Field Operation and Manipulation, Software Package, [Online]. Available: http://www.openfoam.com

[10] B. Aupoix, and P. R. Spalart, "Extensions of the Spalart–Allmaras turbulence model to account for wall roughness," *International Journal of Heat and Fluid Flow*, vol. 24, no. 4, pp. 454-462, 2003.

[11] G. A. Ruff, and B. M. Berkowitz, "Users Manual For the NASA Lewis Ice-accretion Prediction Code (LEWICE)," *NASA*, pp. 55-58, CR-185129, 1990.

[12] F. Morency, F. Tezok, and I. Paraschivoiu, "Anti-icing system simulation using CANICE," Journal of Aircraft, vol. 36, no. 6, pp. 999-1006, 1999.

[13] P. Giguère and M.S. Selig, "Design of a Tapered and Twisted Blade for the NREL Combined Experiment Rotor," NREL, 1999, NREL/SR-500-26173.

[14] N. N. Sørensen, J. A. Michelsen, and S. Schreck, "Navier–Stokes predictions of the NREL phase VI rotor in the NASA Ames 80 ft× 120 ft wind tunnel," Wind Energy: An International Journal for Progress and Applications in Wind Power Conversion Technology, vol. 5 issue, 2-3, pp. 151-169, 2002.

[15] C. M. Langel, R. Chow, and C.P. van Dam, "A Transport Equation Approach to Modeling the Influence of Surface Roughness on Boundary Layer Transition," SANDIA National Laboratories, 2017, SAND2017-10670.